Proc. of SPIE Vol. 3353, Adaptive Optical System Technologies, ed. D Bonaccini, R K Tyson (Jun 1998) Copyright SPIE

Laser guide star simulations for 8-m class telescopes

F. Delplancke[a], M. Carbillet[b], N. Hubin[a], S. Esposito[b], F. Rigaut[a],
E. Marchetti[c], A. Riccardi[b], É. Viard[a], R. Ragazzoni[d], M. Le Louarn[a] and L. Fini[b]

[a]ESO, Karl-Schwarzschild Str. 2, 85748 Garching-bei-Muenchen, Germany

[b]Osservatorio Astrofisico di Arcetri, L.go E. Fermi 5, 50125 Firenze, Italy

[c]Centro Galileo Galilei, Calle Alvarez de Abreu 70, 38700 Santa Cruz de La Palma, Spain

[d]Osservatorio Astronomico di Padova, vicolo dell'Osservatorio 5, 35122 Padova, Italy

ABSTRACT

We describe in this paper the development of a simulation tool for modeling any kind of adaptive optic system with laser guide star within the framework of the European network *Laser Guide Star for 8-m Class Telescopes*. This is intended to support investigations about laser guide stars problems like cone effect and tip-tilt determination. The different kind of software modules to be developed are listed and the libraries already distributed among the network are described: phase screen generation (with fast Fourier transform and Zernike methods), downward propagation (for natural and laser guide stars), wavefront sensing and reconstruction (with Shack-Hartmann and curvature sensor of various geometries). The future studies for solving the cone effect are also presented.

Keywords: adaptive optics, laser guide star, atmospheric perturbations, wavefront sensing, cone effect, atmospheric tomography.

1. INTRODUCTION

For large telescopes (8-m class), the use and performances of adaptive optics (AO) are limited by the sky coverage,[1,2] i.e. the lack of bright enough natural stars to be used as reference sources. An AO system for large telescopes thus requires the generation of artificial reference sources. Up to now, the only viable proposed solution is the laser guide star (LGS). Two types of LGS can be used: one using the Rayleigh scattering in the lower atmosphere (up to ~20 km altitude) of a laser beam, the other using the excitation of sodium atoms in the mesosphere (*Na* layer at ~90 km altitude).

Both solutions are inducing other problems, linked among others to the finite altitude of the artificial star (cone effect)[3] and to the impossibility to measure the tilt as on a natural guide star (NGS).[4] In order to efficiently implement LGS on AO systems, the investigation of the solutions to those problems requires powerful and versatile simulation codes.

Another topic that must also be investigated in AO is the optimal use of the photons coming to the telescope by the study of innovative wavefront sensing techniques. The best use of photons would allow to increase the limiting magnitude of NGS AO and thus to increase the sky coverage or to reduce the necessary laser power.

A *Training and Mobility of Researchers* Network devoted to the study of *Laser Guide Star for 8-m Class Telescopes* was started in Europe, in January 1997 . This European Commission program and the network are described in Sect. 2. One of the tasks of this network is to create a large software library for AO simulations in order to give a useful toolbox for research on the LGS problems and on optimal use of photons. The exact aims of this simulation tool and the description of its contents can be found in Sect. 3.

A complete software package able to model any standard AO system should be delivered for the end of 1998. Then, new softwares modeling advanced structures or new concepts will be progressively added to the package. Up to now a certain number of routines have been developed, related to:

Other author information: (Send correspondence to F.D.)
F.D.: E-mail: fdelplan@eso.org
M.C.: E-mail: marcel@arcetri.astro.it

- Phase screen generation, using either a fast Fourier transform (FFT) method with sub-harmonics adding (SHA) or Zernike polynomials (see Sect. 4).
- Downward propagation, using geometric optics and applied to any number of NGS and LGS (see Sect.5).
- Wavefront sensor geometry, defining square, radial, hexagonal or user-defined geometries (see Sect. 6).
- Wavefront sensing, modeling either a Shack-Hartmann or a curvature sensor (see Sect. 7).
- Wavefront sensor signal computation, evaluating the slopes and/or curvatures of the wavefront (see Sect. 8).
- Wavefront reconstruction, giving the phase of the reconstructed screen (see Sect. 9).
- Data display, I/O and performance estimation (see Sect. 10).

Finally, our future work about cone effect is introduced (see Sect. 11) and conclusions are drawn on the other future applications of our software package (see Sect. 12).

2. THE *LASER GUIDE STAR FOR 8-M CLASS TELESCOPES* TMR NETWORK

Within its Fourth Framework program, the European Community wants to promote the formation of young researchers in sciences and engineering, via its *Training and Mobility of Researchers* (TMR) program. A full description of the TMR program, its purposes, its actions can be found on the European Community Web site at `http://www.cordis.lu/`.

Our LGS network groups the following research teams: *Centre de Recherches Astronomiques de Lyon/Observatoire de Lyon* (France, coordinator), European Southern Observatory, *Instituto de Astrofisica de Canarias* (Spain), *Osservatorio Astrofisico di Arcetri* (Italy), Imperial College of London (United Kingdom), *Max-Planck Institute fuer Extraterrestrische Physik* (Germany), and National University of Ireland - Galway. The LGS-network aims at coordinating the efforts in Europe to produce a comprehensive set of theoretical and experimental studies which are necessary to implement the LGS on the 8-m telescopes (VLT, Gemini, LBT and ORM in which European countries are implied). Several problems have to be addressed before the LGS implementation. They concern the correction for image wandering (the "tilt" of the incoming wavefront), the "cone effect" due to the parallax between the sodium LGS at ~90 km and the program object, the implementation effects on observations at the telescope and at other telescopes on the site, the specification of the lasers and of their operation mode, as well as the in-depth analysis of the astrophysical requirements. Each of these problems is approached as follows. A theoretical analysis of the problem is performed, based on a common simulation code. Then, when appropriate, experiments at lab and onto the sky are built, operated and analyzed. The ultimate goal of the program is to deliver specifications of the LGS as optimal as possible. The tasks are dispatched between five workpackages (WP). The first one investigates the scientific programs which can ultimately be done with LGS on 8m telescopes, accounting for the technical constraints (i.e.: tilt correction and field). The aim of the second WP is to produce a code for simulating the ensemble atmosphere-telescope-AO-LGS, to model different AO systems or LGSs. This is the object of the present paper. The third WP takes care of operational issues. Safety and light pollution studies must be concluded before operating a LGS. Laser type and configuration, laser operation and maintenance, and astronomical operation issues are currently investigated. The fourth WP studies advanced wavefront sensing for tilt measurement, field increase and better use of photons. The fifth WP gives experimental feedback to the precedent theoretical studies by using AO and LGS on real telescopes, by measuring seeing vertical distributions, by making experiments with polychromatic guide stars. More details can be found on the Web site `http://www-obs.univ-lyon1.fr/~tmr-lgs/`.

We shall now describe in more details the second workpackage.

3. SIMULATION PACKAGE DEVELOPMENT

3.1. Aims of the Software Package

The general aim of our work is to develop a complete software library of any possible element of an AO LGS system. This library will, at first, include known classical elements, like Shack-Hartmann or curvature wavefront sensors. Later on it will also incorporate software modeling new elements and advanced, complex phenomena, like the different solutions proposed for the cone effect.

Thus, the structure of the software library should allow the largest versatility to the user in order to test any combination of elements, to search for optimal configurations, to model any partial or end-to-end complex system and to adapt easily to newly developed software. In order to satisfy this requirement, the basic elements of the software library should be as "atomic" as possible, representing an elementary process of the system: the deformable mirror, the tip-tilt mirror, the wavefront sensor, the reconstructor, etc. The atomic element must keep a physical meaning. They have also to be compatible to each other so that they can be plugged together to form larger structures. Moreover the general structure of the software library should allow to use parallel processing for time consuming simulations.

Software will be written in IDL language within a Unix/Linux environment (SPARC or PC 230 MHz with at least 128 Mb of RAM). The input parameters of the AO system will be provided by the user either interactively through the user interface or in a dedicated file. The output data will be available in FITS format for eventual post-processing with other astronomical software. A full, extensive technical documentation and user manual will also be provided.

3.2. Software Library Structure

The software library will be made of **modules** and **macros** that will be linked together by the **user interface**.

The **modules** correspond to the "atomic" elements and must be stand alone routines, i.e. not requiring to use other non-standard IDL routines. They have to be under an immediately executable format in order to spare processing time. The module size has been chosen in order to increase flexibility and possibility of unusual uses, allowing research work. The outputs of the modules should be the data which can be interesting to display or to store for future analysis (e.g. the sensor image or the incident wavefront). We foresee three different types of modules, according to their purposes: AO modules (which implement computational algorithms), User Interface modules (used to implement user interfaces), and Utility modules (used for I/O and other housekeeping tasks). The list of the proposed modules, ordered as a function of their purposes, is given in Table 1.

The modules can be associated together to make larger structures that we call **macros**. From the implementation point of view a macro is a single program, in the classical sense, built up with the use of modules. Most of them will be made by the user, by means of the user interface but some of them will also be provided directly to the user mainly for initialization and calibration purposes. The list of the proposed macros is given in Table 2.

In order to allow the implementation of easy to use end-to-end simulation applications, a number of modules will be implemented which can be used by developers to create **interactive interfaces** to macro parameters and data with built-in knowledge of the structure of the application and of required data and parameters. This seems to be a necessary condition to allow unexperienced users to manage a simulation experiment without the need to cope with the internal structure of the simulation program itself. Such modules will manage the data input from users and perform all the required checks on data consistency to guarantee, at least to some extent, that the following run can be actually performed.

4. PHASE SCREEN GENERATION

The phase screen generation module is aimed to generate phase screens corrupted by the atmospheric turbulence for the whole LGS AO simulation package. Two methods are available at the moment (a FFT+SHA based one, and a Zernike polynomials based one), but we plan to incorporate also a Karhunen-Loeve and a fractal based methods.

4.1. FFT+SHA method

The implemented FFT+SHA method allows to generate phase screens $\varphi(x, y)$ assuming either a Kolmogorov or a von Kármán spectrum $\Phi_\varphi(\nu_x, \nu_y)$ from which calculate the modulus of $\tilde{\varphi}(\nu_x, \nu_y)$, the Fourier transform of $\varphi(x, y)$.

Assuming the near-field approximation and small phase perturbation,[5] the Kolmogorov spectrum is given by

$$\Phi_\varphi(\nu_x, \nu_y) = 0.0228\, r_0^{-\frac{5}{3}} \left(\nu_x^2 + \nu_y^2\right)^{-\frac{11}{6}}, \tag{1}$$

where r_0 is the Fried parameter. Within the framework of the classical FFT based technique, a Kolmogorov phase screen is obtained by taking the inverse FFT of $\tilde{\varphi}(\nu_x, \nu_y)$, which modulus is obtained by using Eq. 1, and which phase is random uniformly distributed. The obtained phase screens suffer however from the lack of spatial frequencies (ν_x, ν_y)

Table 1. List of the proposed module libraries with their types, parameters, purposes and methods for the user `interface modules`, the **adaptive optics modules**, and the *utility modules*.

Module Library	Method/Purpose/Parameters
`Guide object definition`	Types = NGS, extended, LGS
	Parameters = size, spectral type, magnitude, offset, altitude, ...
`Telescope and common optics`	Parameters = diameter, focal ratio, central obscuration, ...
`Sensor geometry`	Types = square, radial, hexagonal, custom , ...
Phase screen generation	Types = Kolmogorov, von Kármán
	Methods = FFT+SHA, Zernike, Karhunen-Loeve, fractal
Downward propagation	Methods = geometrical, Fresnel, polychromatic
Upward propagation (LGS)	Methods = Fresnel, speckle, ...
Wavefront sensing	Types = Shack-Hartmann, curvature
Tip-tilt sensing	Separate or not
Wavefront estimation	Methods = centroids, curvatures, global wavefront reconstruction, ...
Influence functions	Methods = analytical, numerical, ...
Wavefront reconstruction	Methods = interaction matrix, neural network, ...
Modal filtering	
Time filtering	On tip-tilt sensing or higher order wavefront sensing
	Methods = Proportional-Integrator-Derivator, predictor, ...
Hysteresis	Linked to the mirror deformations
Tip-tilt mirror	Separate or not
Deformable mirror	Types = piezostack, bimorph with various boundary conditions
Laser tools	Parameters = power, Rayleigh scattering, Na layer structure, saturation, ...
Data display	Wavefronts, images, mirror shapes, curves
Data I/O	Types = FITS, HDF
Performance evaluation	Structure function, variance analysis, PSD, ...

Table 2. List of the proposed macro libraries with their methods, purposes or parameters

Macro Library	Method/Purpose/Parameters
Interaction matrix	Methods = zonal, modal
Command matrix	Methods = least square, maximum likelihood, optimal estimation, ...
WFS initialization	Parameters = geometrical parameters of the WFS, ...
WFS calibration	Gives the reference measurements from static aberrations, calibration source, ...
System modes	Mirror, Zernike or Karhunen-Loeve modes
Mode gain determination	Methods = analytical, numerical
Transfer function	Of the global system or of part of it

lower than the inverse of the – necessarily finite – dimension of the simulated array. To compensate from this effect the technique of SHA proposed by Lane *et al.*,[6] which consists in generating additional random frequencies and add their effects to the already sampled frequencies, has been chosen.

In the case of a von Kármán spectrum:

$$\Phi_\varphi(\nu_x, \nu_y) = 0.0228\, r_0^{-\frac{5}{3}} \left(\nu_x^2 + \nu_y^2 + \frac{1}{\mathcal{L}_0^2}\right)^{-\frac{11}{6}}, \tag{2}$$

the same procedure is applied, allowing to reach large values of the desired wavefront outer scale $\mathcal{L}_0$ (anyway if $\mathcal{L}_0$ is already sampled by the FFT, no SHA is needed).

Figure 1 shows an example of phase screen (actually a phase *stripe*, useful for temporal evolution – e.g. in the framework of the downward propagation module of Sect. 5) generated using this method and a von Kármán modulus,

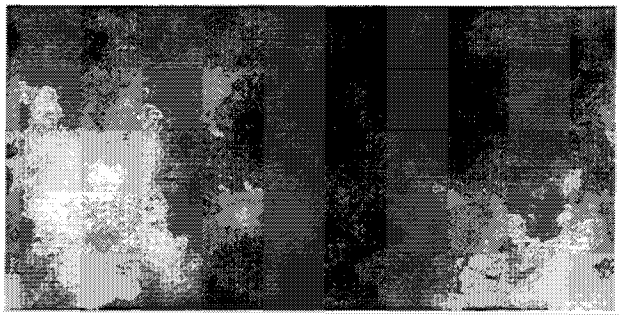

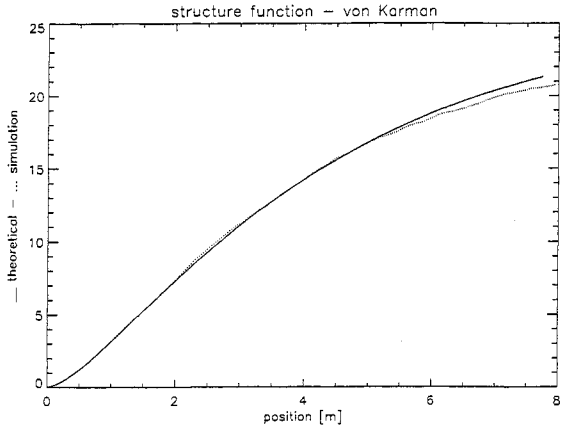

Figure 1. Example of a von Kármán FFT phase stripe, together with the associated theoretical (straight line) and simulated (doted line) structure functions.

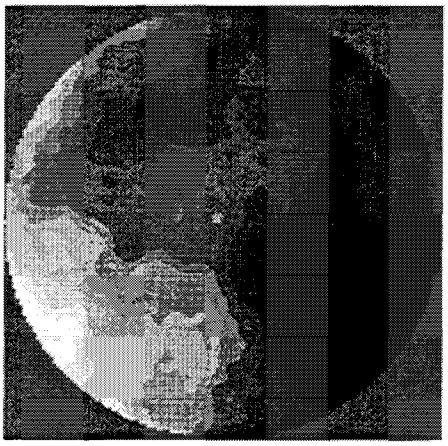

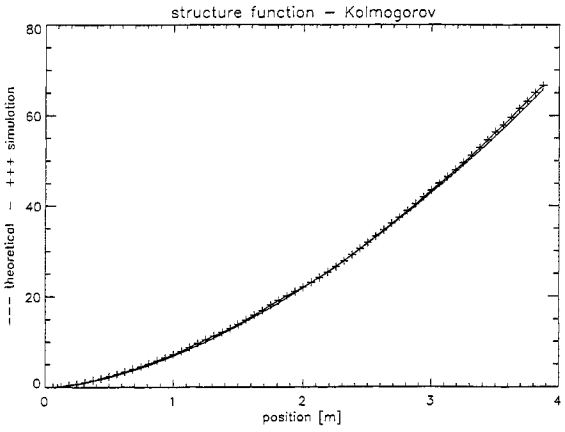

Figure 2. Example of a Kolmogorov Zernike phase screen, together with the associated theoretical (straight line) and simulated (crossed line) structure functions.

together with the associated structure function that shows a very good agreement between theory and simulation. 1000 phase stripes of dimension 1024×512 px (corresponding to 32 m×16 m) were used for this test, with $\mathcal{L}_0$=20 m and r_0=1 m.

4.2. Zernike polynomials method

When the Zernike polynomials method is used, the phase screens are generated as the sum of the first $N = (j_{max} - 1)$ Zernike polynomials $Z_j\left(\frac{r}{R}, \theta\right)$:

$$\varphi(r,\theta) = \sum_{j=2}^{j_{max}} c_j Z_j\left(\frac{r}{R}, \theta\right), \tag{3}$$

where r and θ are the polar coordinates on the pupil of radius R. The piston term (j=1) is not considered because the point spread function (PSF) is not depending on it. For each phase screen realization, an independent set of the

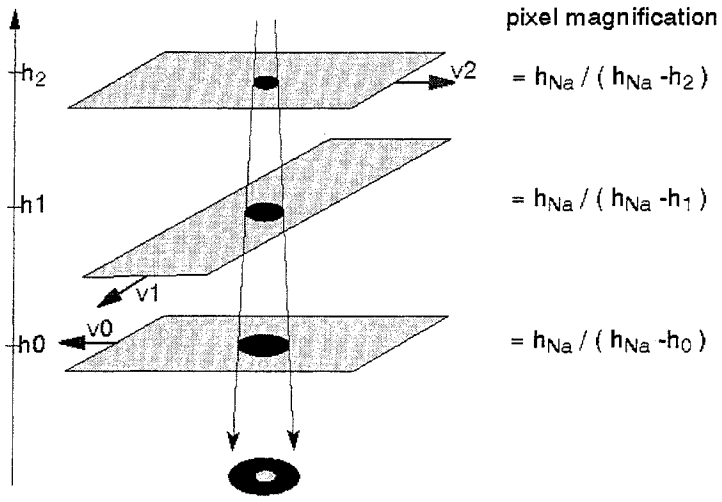

Figure 3. Principle of the 3-layers downward propagation algorithm involving the light scattering back from a sodium LGS.

coefficients c_j is obtained with the correct statistics stated by the $N \times N$ covariance matrix[7]: $C_{j,j'} = \langle a_j a_{j'} \rangle$. Only a small portion of the matrix has non-zero elements, so the sparse matrix algorithms are used to allocate less memory and increase the code speed.[8]

To obtain a good behavior of the phase screens at high spatial frequencies, j_{max} must be large enough to take into account polynomials with a number of oscillations over the pupil diameter comparable to the chosen sampling (usually at least 2 or 3 px per r_0). In these conditions j_{max} can be as large as a few thousands in the visible for 8-m class telescopes. The usual definition formula for the Zernike radial component[9] is not effective to compute polynomials with $j > 1030$ when double precision arithmetic is used. To overcome this problem we developed an algorithm based on an alternate definition for $Z_j(\rho, \theta)$, involving the recurrence definition of the Jacobi polynomials[10] and the relationship between the Zernike and the Jacobi polynomials.[11]

Figure 2 shows an example of phase screen generated using this last method. The structure function (computed from 400 phase screens 256×256 px, i.e. 8 m×8 m, with $j_{max} = 4186$ and $r_0 = 1$ m) is here again in very good agreement with the theoretical one (Kolmogorov here).

In both cases, the output is a number of phase screens (or stripes) suitable for the rest of the simulation modules.

5. DOWNWARD PROPAGATION

The downward propagation module is aimed to propagate the phase through up to three turbulent layers of the atmosphere down to the telescope pupil. To each of these layers is affected a phase screen previously generated as described in Sect. 4.1, together with an altitude h_i (with $i = 1, 2, 3$), a wind speed v_i, and a relative weight determined with respect to the integrated C_n^2 profile. The three directions of the winds are fixed (see Fig. 3).

Two cases are taken into account at the same time: the sodium LGS one and the NGS one. In the NGS case, the layers' phase screens are simply added in order to obtain the resulting propagated phase perturbations at the telescope pupil. In the sodium LGS case, one has to take into account the altitude h_{Na} of the sodium layer scattering the LGS with respect to the turbulent layers' ones h_i. This results in a pixel magnification (by a factor $\frac{h_{Na}}{h_{Na}-h_i}$) for the phase screens before their adding.

The output is a number of pupil screens (following the kind of temporal evolution chosen) for each Guide Star (see Fig. 4), which parameters are: the type (Natural or Laser), the off-axis angle, and the position angle.

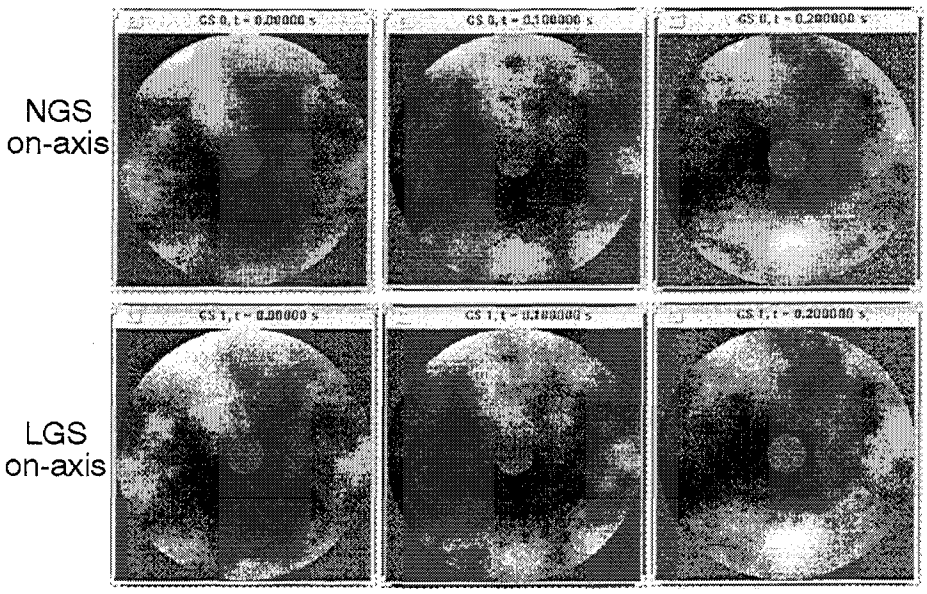

Figure 4. Example of propagated screens vs time evolution. The evolving screens are computed for two different cases corresponding to an on-axis NGS and on-axis sodium LGS. The evolution time is here 0.1 s.

6. WAVEFRONT SENSOR GEOMETRY

The wavefront sensing (WFS) geometry definition has been separated from the wavefront sensing modules because any kind of sensor geometry (square, radial, etc.) can be used with any kind of sensor: curvature, Shack-Hartmann, etc. The classical associations Shack-Hartmann–square or curvature–radial are not always required. It could be useful to make other associations or to use other kinds of sensor geometry and to compare their respective performances related to noise propagation, sensitivity, redundancy, etc.

Three main classical geometries are implemented: square, radial and hexagonal (not yet developed). A custom geometry can also be given by the user. The parameters of those geometries are described below.

These modules compute the geometrical parameters needed for the wavefront sensing modules from the physical parameters entered by the user. Their outputs must be compatible with the Shack-Hartmann and with the curvature modules. The input parameters common to all the geometries are: the size of the simulation (in sampling points, corresponding to the size of the phase screens to be analyzed), the size of the pupil (in meters and in sampling points), the size of the wavefront sensor in sampling points (which can be smaller or bigger than the pupil but smaller than the simulation size) and the wavelength at which the wavefront sensing is operated.

6.1. Squared Geometry

The user gives, as particular inputs, the linear number of subapertures under the pupil and the subaperture size in arcsec. The program adjusts the number of sampling points in order to have it integer under each subaperture, determines which sub-apertures are active (i.e. receive a large enough number of photons), computes their positions, and makes an image of the sensor. Moreover, if it is associated with a Shack-Hartmann wavefront sensor, some rebining process is needed in order that an integer number of sampling points corresponds to one physical pixel of the camera. The module prepares the parameters for this operation. This adjustment is not needed in case of a curvature sensor where the intensity over the full subaperture is detected as a whole. An example of the sensor image is given in Fig. 6.

6.2. Radial Geometry

Here the user can give the data on two ways. Either he is giving only the number of rings and the number of subapertures for each ring, and the program helps him to build a radial sensor with subaperture of equal surfaces

(standard configuration). Or the user gives, in an ASCII file, all the parameters needed to construct the sensor: the inner and outer diameters of each ring, the number of subapertures for each ring and the angular orientation of the first subaperture of each ring relative to a reference direction. An example of such a radial sensor is given in Fig. 7. The program computes the position of each active subaperture and the image of the active sensor.

6.3. Custom Geometry

The user can also introduce any kind of sensor geometry by giving the map of the sensor: an image where one places zeros out of the sensor and pupil and a number corresponding to each subaperture under this one. The program then computes the positions of each subaperture and, for the Shack-Hartmann, prepares the parameters of the rebining in order to have an integer number of sampling points per physical pixel of the camera.

7. WAVEFRONT SENSING

The wavefront sensing modules firstly take the wavefront corrected by the deformable mirror, secondly add the possible static aberrations of the common optics, and finally compute the image(s) coming out of the wavefront sensor. In the case of the Shack-Hartmann, it gives one image composed of the images of each sub-aperture, rebined according to the pixel size of the WFS camera. In the case of the curvature sensor, it gives a set of extra-focal images.

7.1. Shack-Hartmann Wavefront Sensor

A scheme of the SHWFS principle is given in Fig. 5. From the wavefront incident on the pupil, the program extracts the parts arriving on each subaperture and computes the images made by these ones. Then it takes their intensity and, in case of extended reference object or calibration source (e.g. an optical fiber), convolves it with the image of this object. It applies the sky background noise (except with the fiber calibration source) and rebins the sampling points to the camera pixels. The result is normalized and converted in number of photons. Finally, the photon and read-out noises are applied if required. A threshold can also be applied if asked by the user. All the subaperture images are gathered in a general wavefront sensing image, which is the output of this module.

7.2. Curvature Wavefront Sensor

A scheme of the CWFS principle is given in Fig. 5. This module can handle the case of a vibrating membrane where the extra-focal domain is scanned sinusoidally. But one cannot take an infinite number of extra-focal images. Thus the user has to discretize the scanning domain into a number n of sampling points where the images will be computed. Usually, about 10 sampling points within one period give a good approximation of reality. For the extra-focal plane i, the defocus is a quadratic function of the distance L_i given by:

$$L_i = \pi\lambda f \frac{f-l}{l} \sin(\frac{i2\pi}{n}), \tag{4}$$

where l is the distance of the extra- or intra-focal plane the closest to the focus, f is the focal length of the telescope and common optics, and λ is the WFS wavelength. For each point, the pure defocus wavefront is computed and convolved with the wavefront to be analyzed. This defocused phase screen is imaged again on the sensor lenslet array. The intensity of this image is computed, convolved with the possible extended reference or calibration object, normalized, and converted into the corresponding number of photons. The sky background is added. It is considered to be equally distributed on all the subapertures. The obtained images (for each extra-focal distance) are stored in an image cube, the output of this routine.

8. WAVEFRONT SENSOR SIGNAL COMPUTATION

The WFS signal computation modules have to convert the wavefront sensor images into the numerical signals representing some of the wavefront characteristics. For instance, from the Shack-Hartmann image, one can calculate the centroid positions of the subpupil images. From the curvature images, one can calculate the classical differential signal under each subaperture, which is linked to the curvatures and slopes of the wavefront. But other methods could be used, like the global wavefront reconstruction (using the full image characteristics and not only the first or second order terms), or like the asymmetric algorithm for the curvature sensor (which allows to retrieve the shape of the extended object). Presently, only the slope estimator for the SHWFS (centroiding) and the classical symmetric algorithm for the CWFS are implemented. They are described here below.

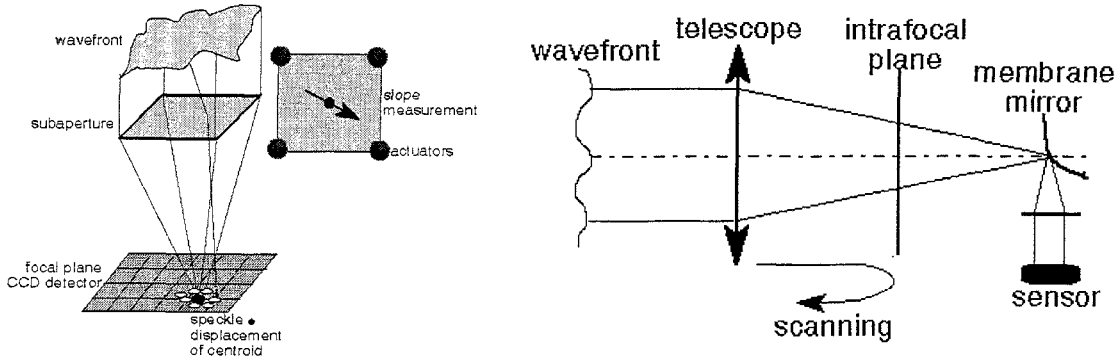

Figure 5. Principle scheme of the Shack-Hartmann wavefront sensor (under one of the subapertures) at left and of the curvature wavefront sensor (with a vibrating membrane) at right.

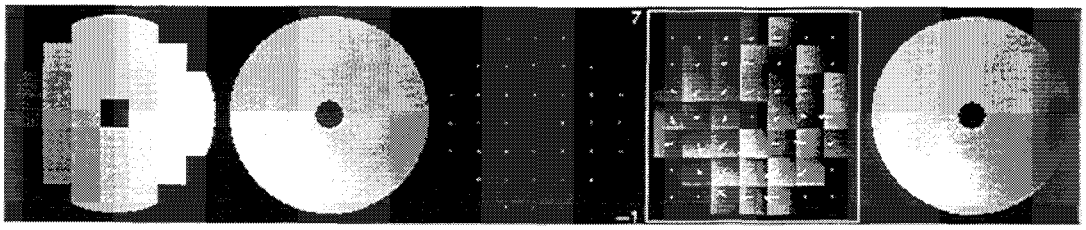

Figure 6. Example of the results obtained with the modeling of a Shack-Hartmann wavefront sensor (7×7 subapertures of 2.18 arcsec, pixel size = 0.136 arcsec, read-out noise = 10 e^- rms, point-like NGS of magnitude 3). From left to right: the WFS geometry map, the incident wavefront (Kolmogorov phase screen), the SHWFS image, the corresponding slopes (represented as facets and arrows), and the reconstructed wavefront (zonal, Fried geometry).

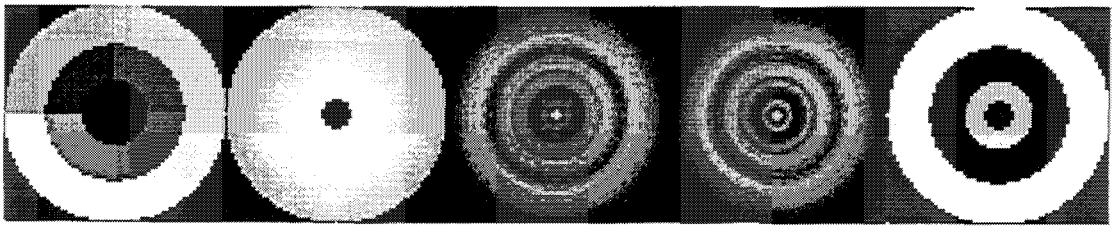

Figure 7. Example of the results obtained with the modeling of a curvature wavefront sensor (3 rings with 1, 4 and 8 subapertures of equal area, extra-focal distance = 30 cm, scanning with 5 sampling points in the extra-focal plane, noise implemented; point like NGS of magnitude 5). From left to right: the WFS geometry map, the incident wavefront (pure defocus), two symmetrical intra- and extra-focal images, and the image of the CWFS signals.

8.1. Centroid Estimator

Each subaperture image is extracted from the image given by the Shack-Hartmann wavefront sensing module. The position (in camera pixels) of its centroid is computed and then the centroid position coming from the calibration measurements is subtracted in order to give the real decentering due to the wavefront aberrations. If the subaperture does not receive enough flux, its signals is set at a reference zero value. The centroid position can then be converted in real wavefront slopes with the appropriate factor. It is required only when one wants to reconstruct the wavefront; in closed loop, the centroids can be used directly. So this operation is placed outside of this module. An example of the results that can be obtained is given in Fig. 6.

8.2. Curvature and Slope Estimator for the CWFS

This module takes the image cube coming out of the curvature wavefront sensing module, adds the intra-focal images on one side and the extra-focal images on the other side. The intra- and extra-focal are computed by integrating the image intensity under each subaperture. The photon noise is then added, if requested by the user. Finally, the differential signal is computed using the following equation:

$$S = \frac{S_{intra} - S_{extra}}{(1-G)S_{old} + G(S_{intra} + S_{extra})}, \tag{5}$$

where S_{intra} and S_{extra} are the intra- and extra-focal signals on the considered subaperture, G is the gain of running average and S_{old} is the denominator of Eq. 5 at the previous iteration. If G is set to 1, one finds back the usual curvature sensing equation for the differential signal. The signals obtained during the calibration process have then to be subtracted from the measured values. If a subaperture does not receive any photon, the signal is set to zero. An example of the results that can be obtained is given in Fig. 7.

9. WAVEFRONT RECONSTRUCTION

For the wavefront reconstruction, we have the choice between the direct zonal reconstruction from the slopes or/and the curvatures, and the reconstruction through modes, which allows to filter them. The latter requires to choose a set of modes: Zernike, Karhunen-Loeve or mirror modes. Zonal reconstruction can be implemented directly and depends only on the geometry on which one wants to reconstruct.[12–14] Up to now, the zonal reconstruction based on Fried geometry,[12] with a least square algorithm has been implemented but the modal methods will be developed as soon as possible. For the curvature sensing, the Poisson equation with the Neumann boundary conditions has to be solved for the direct reconstruction.[15,16]

10. SYSTEM PERFORMANCES, DATA DISPLAY AND I/O

Several modules have been developed in order to display the incident wavefront, the sensor image(s), the sensor signals, the reconstructed wavefront and the wavefront structure function. They can be plugged simply after the modules giving the corresponding data and displaying the images at the requested positions, with the requested sizes, as demonstrated in Fig. 6 and Fig. 7. The other modules will be developed as a function of the needs of the other module libraries.

11. WORK IN DEVELOPMENT - FUTURE WORK

A major difficulty with LGS is the cone effect which is due to the slight difference between the conical propagation path of the laser beam and the cylindrical path of the stellar beam.

In order to correct the cone effect, multiple LGS systems can be used. Different methods with multiple LGS have been studied either using 2-D reconstruction (stitching[17] and merging[18] methods) or 3-D reconstruction (tomography methods[3,19,20]).

The difference between stitching and merging is the fact that the subapertures measure the wavefront from all LGSs in the merging method whereas, in the stitching method, each subaperture senses only one spot and the boundaries of adjacent spots, as illustrated in Fig. 8. Sasiela[17] and Tyler[18] have described these methods, but did not provide detailed algorithms to perform the wavefront reconstruction.

The tomographic method permits to reconstruct the phase corrugations of each turbulent layer using matrix inversion methods. Tallon and Foy,[3] Jankewicks *et al.*[19] have explained possible 3-D reconstructions.

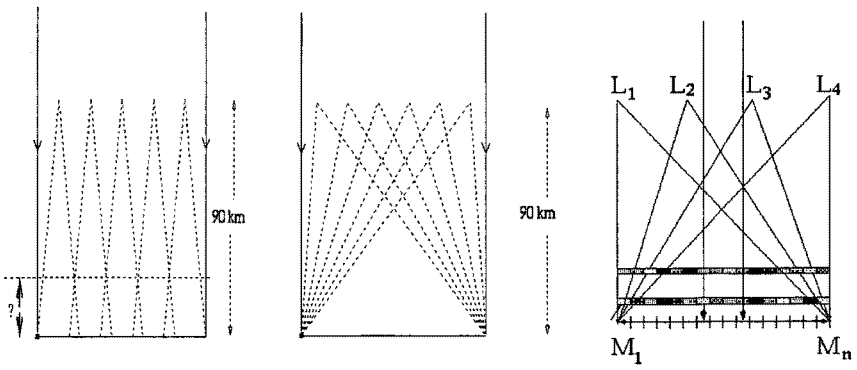

Figure 8. Principle schemes of the stitching, merging and tomography methods for solving the cone effect.

These 3-D reconstruction methods are based on the fact that generally, in astronomical sites, turbulence is concentrated in a few (2 to 5) thin turbulent layers. Assuming that one knows the height and number of these layers (for example by using SCIDAR techniques), one can, by solving a set of linear equations, reconstruct the phase aberrations in each of these layers. Multiple deformable mirrors can then be used to correct each layer separately in their optically conjugated planes. This allows one to solve the cone effect and also to increase dramatically the corrected AO field of view. A simulation of this method has been realized and the results are being analyzed. Several inversion methods are being investigated. The geometry of the laser spots, and their number are also being investigated. A laboratory experiment, realized at *Centre de Recherches Astronomiques de Lyon*, has also been made, in order to simulate real measurements and to check the validity of computer simulations. This experiment includes phase screens to simulate atmospheric turbulence, and an array of micro-lenses to measure the produced phase aberrations. Results of this experiment are also being analyzed.

12. CONCLUSIONS

In this paper have been presented the aims, the results and the future works of the European network *Laser Guide Star for 8-m Class Telescopes* in the field of developing a software package in order to modelize any type of AO system, simple or complex, end-to-end or partial, with or without LGS. At first, the package will cover all the AO sub-systems whose theory has already been developed. Then new modules will be added as a function of the advanced researches made in the network. The first basic package will be completed by the end of 1998.

Up to now, the developed modules include: phase screen generation (with FFT and SHA or with Zernike polynomials), downward propagation (geometrical optics, for any number of LGS and NGS), wavefront sensor geometry definition (square, radial, hexagonal or custom), wavefront sensing (Shack-Hartmann or curvature), wavefront estimation (centroiding or curvature and slopes), wavefront reconstruction (zonal with Fried geometry), several data display, I/O and performance estimations. These routines have been described in more details with their assumptions, parameters, methods, inputs and outputs.

The future software investigations will concern: advanced wavefront sensors for a better use of photons, advanced modal control, advanced reconstruction methods, flexible time and modal filtering for tip-tilt and higher orders, cone effect with multispot LGS, Rayleigh scattering, LGS spot elongation, *Na* layer saturation effects, tip-tilt solving via polychromatic LGS and perspective methods.

There is still a lot of work to be done but our goal is, at term, to provide the scientific community with a powerful, flexible, versatile and easy-to-use software package for AO LGS simulations.

ACKNOWLEDGMENTS

The authors gratefully acknowledge the financial support of the European Community, through the *Training and Mobility of Researchers* program network, under contract number ERBFMRX-CT96-0094.

REFERENCES

1. M. L. Louarn, R. Foy, N. Hubin, and M. Tallon, "Laser guide star for 3.5- and 8-m telescopes : performances and astrophysical implications," *MNRAS* **295**, pp. 756–763, 1998.
2. M. L. Louarn, N. Hubin, R. Foy, and M. Tallon, "Sky coverage and psf shape with lgs ao on 8-m telescopes," in *Adaptive Optical System Technologies*, D. Bonaccini and R. K. Tyson, eds., *Proc. SPIE* **March 1998**, pp. paper 3353–99, 1998.
3. M. Tallon and R. Foy, "Adaptative telescope with laser probe: isoplanatism and cone effect," *Astron. Astrophys.* **235**, pp. 549–557, 1990.
4. F. Rigaut and E. Gendron, "Laser guide star in adaptive optics - the tilt determination problem," *Astron. Astrophys.* **261**, pp. 677–684, 1992.
5. F. Roddier, "The effects of atmospherical turbulence in optical astronomy," *Progress in Optics* **19**, pp. 283–375, 1981.
6. R. G. Lane, A. Glindeman, and J. C. Dainty, "Simulation of a kolmogorov phase screen," *Waves in Random Media* **2**, pp. 209–224, 1992.
7. N. Roddier, "Atmospheric wavefront simulation using zernike polynomials," *Opt. Eng.* **29**, pp. 1174–1180, 1990.
8. W. H. Press, B. P. Flannery, S. A. Teukolsky, and W. T. Vetterling, *Numerical Recipes in* C, Cambridge University Press, Cambridge, 1986.
9. R. Noll, "Zernike polynomials and atmospheric turbulence," *J. Opt. Soc. Am.* **66**, pp. 207–211, 1976.
10. W. Magnus, F. Oberhettinger, and R. P. Soni, *Formulas and Theorems for the Special Functions of Mathematical Physics*, Springer Verlag, Berlin, 1966.
11. M. Born and E. Wolf, *Principles of Optics*, Pergamon, New York, 1985.
12. D. L. Fried, "Least-square fitting a wavefront distorsion estimate to an array of phase-difference measurements," *J. Opt. Soc. Am.* **67**, pp. 370–375, 1977.
13. W. H. Southwell, "Wavefront estimation from wavefront slope measurements," *J. Opt. Soc. Am.* **70**, pp. 998–1006, 1980.
14. R. K. Tyson, *Principle of Adaptive Optics 2nd edition*, Academic Press, Boston, 1993.
15. F. Roddier, "Curvature sensing and compensation: a new concept in adaptive optics," *Appl. Opt.* **27**, pp. 1223–1225, 1988.
16. F. Roddier, "Wavefront sensing and irradiance transport equation," *Appl. Opt.* **29**, pp. 1402–1403, 1990.
17. R. J. Sasiela, "Wavefront correction by one or more synthetic beacons," *J. Opt. Soc. Am. A* **11**, pp. 379–393, 1994.
18. G. A. Tyler, "Merging: a new method for tomography through random media," *J. Opt. Soc. Am. A* **1**, pp. 409–424, 1994.
19. A. J. Jankevics and A. Wirth, "Wide field of view adaptive optics," in *Active and Adaptive Optical Components*, M. E. Ealey, ed., *Proc. SPIE* **1543**, pp. 438–448, 1991.
20. J. M. Beckers, "Increasing the size of the anisoplanatic patch with multiconjugate adaptive optics," in *Very Large Telescopes and Their Instrumentation*, M. H. Ulrich, ed., *Proc. ESO conference* **March 1988**, pp. 693–703, 1988.